

Improved particle tracking velocimetry based on level set segmentation for measuring the velocity field of granular flow

Jing-Yi Gao(高靖宜), Quan Chen(陈泉), Ran Li(李然), Ge Sun(孙歌), Tong-Tong Mu(牟彤彤), and Hui Yang(杨晖)

Citation : Chin. Phys. B, 2025, 34 (**2**): 024201. DOI: 10.1088/1674-1056/ad989a
Journal homepage: http://cpb.iphy.ac.cn; http://iopscience.iop.org/cpb

What follows is a list of articles you may be interested in

High-quality ghost imaging based on undersampled natural-order Hadamard source

Kang Liu(刘炕), Cheng Zhou(周成), Jipeng Huang(黄继鹏), Hongwu Qin(秦宏伍), Xuan Liu(刘轩), Xinwei Li(李鑫伟), and Lijun Song(宋立军)

Chin. Phys. B, 2024, 33 (**9**): 094204. DOI: 10.1088/1674-1056/ad62e1

Design of a high sensitivity and wide range angular rate sensor based on exceptional surface

Xinsheng Ding(丁鑫圣), Wenyao Liu(刘文耀), Shixian Wang(王师贤), Yu Tao(陶煜), Yanru Zhou(周彦汝), Yu Bai(白禹), Lai Liu(刘来), Enbo Xing(邢恩博), Jun Tang(唐军), and Jun Liu(刘俊)

Chin. Phys. B, 2024, 33 (**8**): 084204. DOI: 10.1088/1674-1056/ad4324

Comprehensive study of the ultrafast photoexcited carrier dynamics in Sb_2Te_3-GeTe superlattices

Zhijiang Ye(叶之江), Zuanming Jin(金钻明), Yexin Jiang(蒋叶昕), Qi Lu(卢琦), Menghui Jia(贾梦辉), Dong Qian(钱冬), Xiamin Huang(黄夏敏), Zhou Li(李舟), Yan Peng(彭滟), and Yiming Zhu(朱亦鸣)

Chin. Phys. B, 2024, 33 (**7**): 074210. DOI: 10.1088/1674-1056/ad432a

Improved spatial filtering velocimetry and its application in granular flow measurement

Ping Kong(孔平), Bi-De Wang(王必得), Peng Wang(王蓬), Zivkovic V, Jian-Qing Zhang(张建青)

Chin. Phys. B, 2020, 29 (**7**): 074201. DOI: 10.1088/1674-1056/ab8ac2

A novel particle tracking velocimetry method for complex granular flow field

Bi-De Wang(王必得), Jian Song(宋健), Ran Li(李然), Ren Han(韩韧), Gang Zheng(郑刚), Hui Yang(杨晖)

Chin. Phys. B, 2020, 29 (**1**): 014207. DOI: 10.1088/1674-1056/ab5936

Improved particle tracking velocimetry based on level set segmentation for measuring the velocity field of granular flow

Jing-Yi Gao(高靖宜)[1,2], Quan Chen(陈泉)[1], Ran Li(李然)[1], Ge Sun(孙歌)[1,2], Tong-Tong Mu(牟彤彤)[1,2], and Hui Yang(杨晖)[2,†]

[1] *School of Optical-Electrical and Engineering, University of Shanghai for Science and Technology, Shanghai* 200093, *China*
[2] *School of Medical Instruments, Shanghai University of Medicine & Health Sciences, Shanghai* 201318, *China*

(Received 11 July 2024; revised manuscript received 28 October 2024; accepted manuscript online 29 November 2024)

Using traditional particle tracking velocimetry based on optical flow for measuring areas with large velocity gradient changes may cause oversmoothing, resulting in significant measurement errors. To address this problem, the traditional particle tracking velocimetry method based on an optical flow was improved. The level set segmentation algorithm was used to obtain the boundary contour of the region with large velocity gradient changes, and the non-uniform flow field was divided into regions according to the boundary contour to obtain sub-regions with uniform velocity distribution. The particle tracking velocimetry method based on optical flow was used to measure the granular flow velocity in each sub-region, thus avoiding the problem of granular flow distribution. The simulation results show that the measurement accuracy of this method is approximately 10% higher than that of traditional methods. The method was applied to a velocity measurement experiment on dense granular flow in silos, and the velocity distribution of the granular flow was obtained, verifying the practicality of the method in granular flow fields.

Keywords: granular flow, particle tracking velocimetry, optical flow method, speed, level set segmentation

PACS: 42.30.–d, 47.11.–j, 47.57.Gc

DOI: 10.1088/1674-1056/ad989a **CSTR:** 32038.14.CPB.ad989a

1. Introduction

Granular flows are common in nature as well as in industrial and agricultural production, such as in debris flows,[1] mixing and processing of materials in the pharmaceutical industry,[2] and pipeline transportation of granular materials in engineering.[3] However, the fluid dynamics involved in granular flow phenomena are not fully understood.[4] To better understand these phenomena, with the measurement of the velocity field in dense granular flow systems being the most critical aspect, granular flow measurement technology has advanced rapidly in recent years.[5] Because of the high particle density and complex movements in dense granular flows, the development of new measurement techniques to accurately capture particle velocities remains a significant research challenge. The flow of granules in silos is a typical example,[6–8] and many researchers have conducted studies in this area.

Particle tracking velocimetry (PTV) is a noncontact measurement technique used to determine particle velocities by tracking and matching their positions in two image frames.[9] The main challenge in PTV is accurately matching the particles. Traditionally, differently colored particles have been added to distinguish between the flow particles during the measurement.[10] While this method appears simple, it is difficult to implement because an incorrect number of particles can affect the results. To address these issues, Sielamowicz[11] proposed the use of optical flow technology to measure the velocity of silo particles. The first experiment he conducted using this method was to measure grain particle velocities during the unloading of a two-dimensional flat-bottomed silo. This study obtained both the velocity distribution of the entire field and the schematic trajectory of the flowing particles. Later, his team[12] conducted further experiments to measure particle velocities during the unloading of a wedge-shaped funnel, similar in shape to the exit of a conical silo, and used the optical flow method to determine the boundaries between the flow and stagnation regions. However, this method lacks accuracy in estimating large displacements at the silo's exit and is unclear when measuring the motion velocity boundaries. To address this problem, Wang[13] measured the velocity field of black glass particles during the unloading of a 2D flat-bottomed silo using an improved LK pyramid optical flow PTV method, which reduced the large displacement detection errors through multiscale iterations using pyramid layers.[14,15] However, because the particles in a silo fall under gravity and exhibit complex rheological characteristics ranging from quasi-static to fast and slow flows corresponding to the sidewall area, outlet area, and area above the outlet, the velocity distribution in the silo is uneven, especially near the outlet. Although the above methods perform well in uniform flow fields,[16] they may cause significant errors owing to oversmoothing in non-uniform flow fields.

†Corresponding author. E-mail: yangh_23@sumhs.edu.cn

© 2025 Chinese Physical Society and IOP Publishing Ltd. All rights, including for text and data mining, AI training, and similar technologies, are reserved.

To address non-uniform flow fields, Lu[17] proposed a PIV variational optical flow method based on velocity field segmentation to measure hypersonic flow fields. This method uses level set segmentation to divide the image according to the fluid velocity distribution and establishes segmented smooth constraint conditions in each region based on the assumption of continuous velocity changes. It has higher accuracy for strong velocity gradient boundaries, such as shock waves in hypersonic flows, and is more robust against noise than traditional variational optical flow methods. Yang[18] introduced a new 3D optical flow method based on volume segmentation to estimate fluid flow velocities. This method segments particle volumes using a local level set method based on velocity distribution, providing higher accuracy than the 3D global optical flow method.

The methods described above effectively reduce the impact of non-uniformity in the flow field on velocity measurement by segmenting and identifying different regions based on the characteristics of the segmented smoothing constraints. Inspired by these methods, this paper proposes a particle tracking velocimetry method that incorporates level set segmentation. Recognizing the uneven distribution of the velocity fields, we employed an improved optical flow PTV method combined with level set segmentation to measure the velocity distribution of the particles during silo unloading. Segmental smoothing constraints were established based on the velocity distribution. Verified in complex flow fields, the results show that this method has a higher accuracy than traditional optical flow methods. Additionally, experimental measurements in a three-dimensional silo reveal that this method not only captures a particle velocity distribution like traditional algorithms but also identifies vortex motion in the area above the outlet.

2. Improved optical flow particle tracking velocimetry algorithm

2.1. Fundamentals of particle tracking velocimetry

PTV is a noncontact analytical measurement technique[9] that obtains the velocity of particles by tracking and matching the position information of the particles in two frames. The basic principle of this method is to reflect the motion state of the particles by tracking the position coordinates of the same particle at different moments.[19] The method has two main steps: particle recognition and particle tracking.

The principle of PTV used in this paper is shown in Fig. 1, in which a certain particle A is located at the position (x_1, y_1) in the figure at the time t_1, and after moving over a time interval of Δt, it is located at the position (x_2, y_2) in the figure at t_2, where $\Delta t = t_2 - t_1$. Two consecutive frames of the image are analyzed and the displacements ΔX and ΔY of the particles in the horizontal and vertical directions, respectively, are obtained from the measurements, and the velocity components in the different directions are computed. The equations for the velocity components U and V in the horizontal and vertical directions, respectively, can be expressed as follows:

$$\begin{cases} U = \dfrac{\Delta X}{\Delta t} = \dfrac{x_2 - x_1}{t_2 - t_1}, \\ V = \dfrac{\Delta Y}{\Delta t} = \dfrac{y_2 - y_1}{t_2 - t_1}. \end{cases} \tag{1}$$

Currently, the mainstream implementation of particle tracking measurements involves collecting multiple frames of images taken over short time intervals in sequence and calculating the velocity of the same particle by tracking its position across neighboring frames.

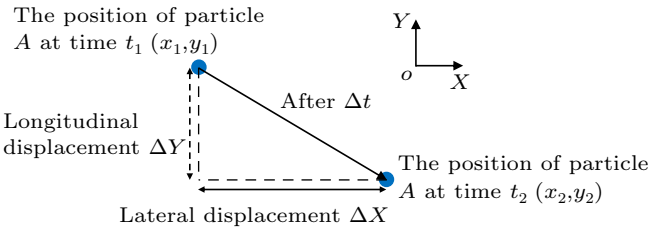


Fig. 1. Schematic of particle tracking principle.

2.2. LK pyramid optical flow method

The LK pyramid optical flow method is an improved particle tracking velocimetry method used in the field of granular flow velocity measurements to obtain the motion of individual particles. The pyramid optical flow method consists of two steps: feature point detection and matching. Figure 2 shows a physical image of corner point detection for discrete particulate matter. If a small change in a pixel at a certain point in an image causes a sudden change in its greyscale value, the pixel is called a corner. In this study, the Shi–Tomasi corner point detection method was used for feature point identification, which has the advantages of high computational efficiency, good anti-noise effect, and robustness. In addition, to overcome the limitation of camera resolution and improve the recognition accuracy of the feature points in the image, the sub-pixel corner point detection method was used to locate the coordinates of the corner points at the sub-pixel level.[20]

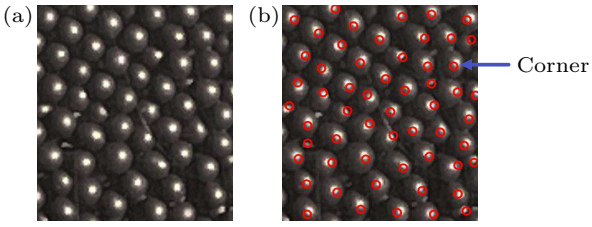


Fig. 2. Tomashi feature detection to extract corner coordinates. (a) The grayscale image of discrete particles, and (b) the image after corner detection.

In image processing, the number of feature points reaches 10^3, which increases the missed detection rate when corner detection is performed on the original image at a single scale.

Therefore, in this study, the layer structure of the image pyramid was added to the corner point detection process; the original image was used as the bottom layer of the pyramid, and multiscale processing was carried out layer-by-layer upward by downsampling. This process can improve the robustness of corner point detection and reduce the false detection rate.[21]

In this study, the Lucas–Kanade pyramid optical flow method (PyrLK) is used for feature point matching in different images. This method uses a pyramidal hierarchical structure to perform multiscale processing on images that can reduce matching errors compared with the traditional matching method and effectively solve the matching problem of large displacements of feature points,[22] which is utilized to perform the matching calculation from top to bottom. In Fig. 3, from top to bottom represents the particle motion reconstruction process from a low sampling rate to a high sampling rate. Under the condition of a low sampling rate, the velocity value of faster particle motion can be calculated accurately, and under the condition of a high sampling rate, the velocity value of slower particle motion can be calculated. The large motion vectors are first identified and then gradually refined, and the deviations of the large motion vectors can be corrected using the small motion vectors.[23]

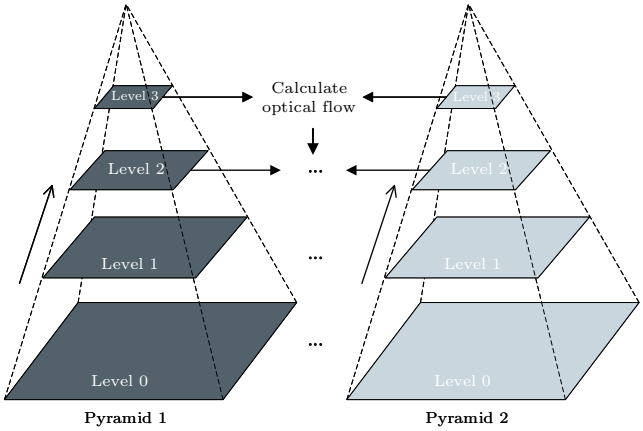


Fig. 3. Optical flow pyramid.

2.3. Level set segmentation

Level set segmentation is a method of segmenting an image based on the geometric metric parameters of the curve contour. It realizes high-precision contour detection by continuously approximating the target boundary through deformable curves and can identify boundaries where the velocity gradient of the complex granular flow varies.[24] The basic idea of this method is to define a level set function in the image domain such that the sub-regions in the image are mapped one-to-one with different values. For more accurate segmentation, the level set function must be continuously adjusted to make the boundary contour position and segmentation shape closer to the real boundary.[25]

Figure 4 shows an image representation of the level set function. In the figure, L_u is the image segmentation boundary; x and y are the coordinates of pixels in the image; $\Phi_u(x,y)$ is the level set function representing the image segmentation boundary, and Ω_u, and Ω_u^{C} are two sub-regions of the image that are complementary to each other. When (x,y) is inside the segmentation boundary L_u, that is, $(xy) \in \Omega_u$, then $\Phi_u(x,y) > 0$. When (x,y) is outside the segmentation boundary L_u, that is, $(xy) \in \Omega_u^{\mathrm{C}}$, then $\Phi_u(x,y) < 0$. When (x,y) is on the segmentation boundary L_u, then $\Phi_u(x,y) = 0$. Therefore, the level set function of image segmentation $\Phi_u(x,y)$ can be expressed as

$$\begin{cases} \Phi_u(x,y) > 0, & (x,y) \in \Omega_u, \\ \Phi_u(x,y) < 0, & (x,y) \in \Omega_u^{\mathrm{C}}, \\ \Phi_u(x,y) = 0, & (x,y) \in L_u. \end{cases} \tag{2}$$

The iteration of the level set function is the key to segmenting the image contours. First, the target image is randomly divided into two sub-regions, $\Omega_{u,1}$ and $\Omega_{u,1}^{\mathrm{C}}$, and the parameters such as the pixel gray gradient, curvature, and mean value of the foreground and background of the image[26] are calculated. The parameter values are then introduced into the following level set function for calculation:

$$\begin{cases} \Phi^{n+1}(x,y) = \Phi^n(x,y) + A(x,y), \\ A(x,y) = 0.2(B(x,y) + C(x,y)), \\ B(x,y) = 6375\delta(\Phi)k + 0.1\delta(\Phi), \\ C(x,y) = \delta(\Phi)\left\{-1\left[u(x,y) - c_1\right]^2 + 0.9\left[u(x,y) - c_1\right]^2\right\}, \end{cases} \tag{3}$$

where $\Phi^n(x,y)$ denotes the value of the level set function at the n-th iteration, $\delta(\Phi)$ denotes the Dirac function, k denotes the contour curvature, $u(x,y)$ denotes the image grayscale, and c_1 and c_2 denote the mean values of the foreground and background.

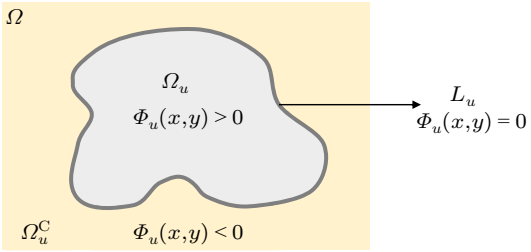


Fig. 4. Expression of level set function.

Formula (3) is used to calculate the value of $\Phi_u^1(x,y)$ and determine whether the function value satisfies formula (2). If the function $\Phi_u^1(x,y)$ satisfies formula (2), the contour of the sub-region $\Omega_{u,1}$ is expanded with a step size of $\lambda = 0.5$ steps to obtain the sub-region $\Omega_{u,2}$, and the level set function $\Phi_u^2(x,y)$ is calculated. If the function $\Phi_u^1(x,y)$ does not satisfy formula (2), the contour of the sub-region $\Omega_{u,1}$ is shrunk with a

step size of $\lambda = 0.5$ steps to obtain the sub-region $\Omega_{u,2}$, and the level set function $\Phi_u^2(x,y)$ is calculated. Next, two conditions are used to determine whether to continue the iteration. Condition 1: the residual threshold of the level set function is calculated as $T_1 = |\Phi_u^1(x,y) - \Phi_u^2(x,y)|$. When the value of T_1 is less than the threshold $T_s = 10^{-5}$, the iteration is stopped. Condition 2: the maximum number of iterations K is set to 100. When the number of evolutionary iterations reaches the maximum, the iteration is stopped. When any of the above conditions is satisfied, the iteration is stopped.[27] In addition, the Dirac function and the Heaviside function are used as auxiliary functions in the process of iteration for calculating the rate of change of the level set function and distinguishing the foreground from the background. According to the iterative evolution described above, the segmentation contour closer to the true boundary is obtained repeatedly.

2.4. Improved optical flow method based on level set segmentation

In granular flow velocity field measurements, oversmoothing occurs when traditional optical flow methods are used to detect regions with large changes in velocity gradients, resulting in large measurement errors near the boundaries of these regions.[28] To solve this problem, level set segmentation was combined with the pyramidal optical flow method in this study to measure the velocity of particle motion in silos. Figure 5 shows the flow chart of the improved optical flow method based on level set partitioning; the four main steps of the method are as follows:

(i) First, the traditional optical flow method is used to detect particle motion and obtain its velocity distribution, including the horizontal and vertical velocity distributions.

(ii) Subsequently, using the level set segmentation method, the vertical and horizontal velocity fields are segmented to obtain the boundary contours of areas with significant velocity gradient changes, and the granular flow is divided into regions according to the boundary contours.

(iii) The pyramid optical flow method is used to detect particle motion in each segmented region and obtain the velocity of the particle motion.

(iv) Finally, the velocities of the particles in each subregion are merged to obtain the velocity distribution of the entire granular flow field.

The above method establishes segmental smoothing constraints through level set segmentation, which avoids oversmoothing in areas with sudden velocity changes, thus obtaining clearer velocity boundaries and effectively preserving the spatial discontinuities of non-uniform flow fields.

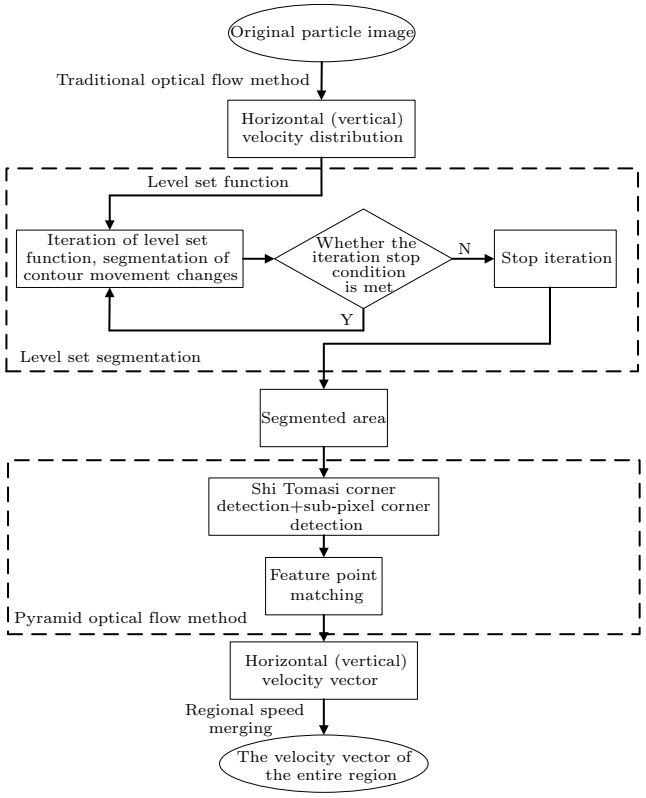


Fig. 5. Flowchart of the level set segmentation optical flow method.

3. Experimental verification through simulations

To verify the accuracy of the improved algorithm, the Euler method[29] was used to simulate the motion of discrete particles. First, discrete particles are randomly generated and the position coordinates of each particle at the initial moment are recorded, then an external force is applied to the particles, and the acceleration of the particle is calculated according to the direction of the force and the existing acceleration of the particles, and the velocity and position coordinates of the particles at the next moment are obtained.[30] The above steps are repeated to obtain the target particle flow field.

3.1. Simulation of a complex granular flow field

Figure 6 shows the particle flow field obtained through simulation using the Euler method. One thousand particles were randomly generated in an area of 1000×700 pixels, and the position of each particle was generated using a uniform random distribution function. The random distribution within the specified area can bring the disordered distribution state of the particles in the flow field closer to the initial conditions in the actual physical environment. The gravitational force acting on the particles was simulated by applying external forces to each particle, which caused the particles to undergo a translational motion with $v_t = 1000$ pixels/s. The coordinates of the particles in the previous frame were $(x_1, y_1) = (x_{t_1}, y_{t_1})$. The

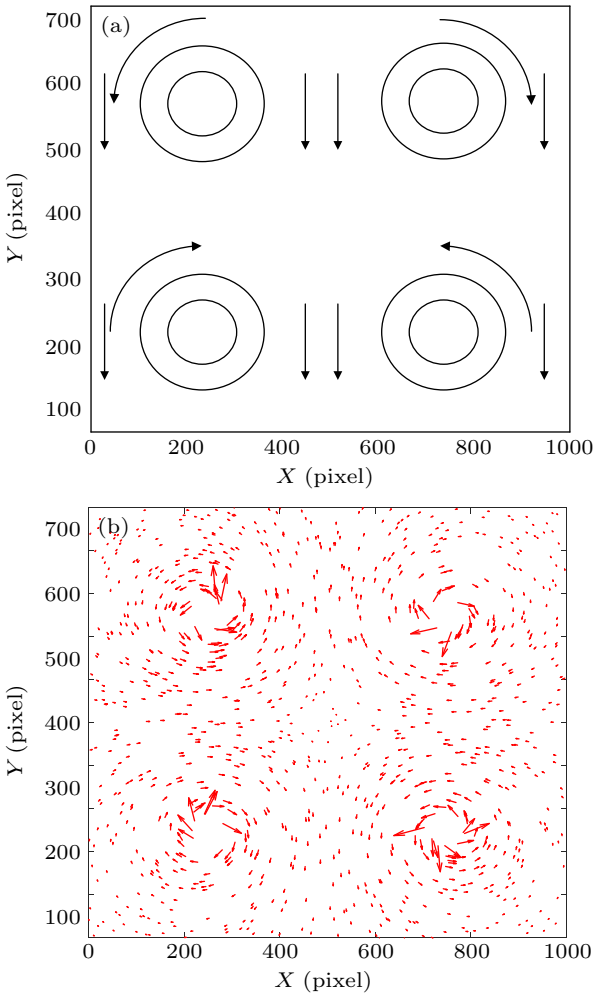


Fig. 6. Flow pattern and vector diagram of particle motion. (a) Flow pattern of particle motion. (b) Vector diagram of particle motion.

formula for translational motion is as follows:

$$x_{t_2} = x_{t_1}, \quad y_{t_2} = y_{t_1} + v_t \cdot \Delta t, \tag{4}$$

where v_t is the velocity component of the particle in the y direction, and Δt is the time step. The particles in the eddy current field were also subjected to another external force, causing them to undergo a rotational motion of $v_r = 2500$ rad/s around the center of rotation. The rotational transformation formula is as follows:

$$\begin{aligned} x_{r_2} &= \left(x_{r_1} - x_{r_0}\right)\cos\left(v_r w \Delta t\right) \\ &\quad \pm \left(y_{r_1} - y_{r_0}\right)\sin\left(v_r w \Delta t\right) + x_{r_0}, \end{aligned} \tag{5}$$

$$\begin{aligned} y_{r_2} &= \pm\left(x_{r_1} - x_{r_0}\right)\sin\left(v_r w \Delta t\right) \\ &\quad + \left(y_{r_1} - y_{r_0}\right)\cos\left(v_r w \Delta t\right) + y_{r_0}, \end{aligned} \tag{6}$$

where (x_{r_0}, y_{r_0}) is the center of rotation, (x_{r_1}, y_{r_1}), (x_{r_2}, y_{r_2}) are the particle coordinates before and after the rotation transformation, Δt represents the time interval, w is a parameter representing the rotation angle, and the positive and negative signs represent the rotation direction.[20] To obtain the overall position of the particles under simultaneous translational and rotational motion, the following formula is used:

$$\begin{aligned} x_2 = x_{t_2} + x_{r_2} &= \left(x_{r_1} - x_{r_0}\right)\cos\left(v_r w \Delta t\right) \\ &\quad \pm \left(y_{r_1} - y_{r_0}\right)\sin\left(v_r w \Delta t\right) + x_{r_0}, \end{aligned} \tag{7}$$

$$\begin{aligned} y_2 = y_{r_2} + y_{t_2} &= y_{t_1} + v_t \Delta t \pm \left(x_{r_1} - x_{r_0}\right)\sin\left(v_r w \Delta t\right) \\ &\quad + \left(y_{r_1} - y_{r_0}\right)\cos\left(v_r w \Delta t\right) + y_{r_0}, \end{aligned} \tag{8}$$

where (x_2, y_2) represents the coordinates of the particles in the frame after motion. The particles underwent simultaneous translational and rotational movements. Using the above formula, the position coordinates of the particles in each frame can be calculated, and the coordinates of all particles in each frame can be iteratively calculated as their true coordinates. Figure 6(b) shows a vector diagram of particle motion at a certain moment. In this simulated flow field, both translational and rotational movements occurred, and the velocity gradient varied significantly, resulting in an uneven distribution of the velocity field. This was consistent with the actual particle motion characteristics and was suitable for verifying the accuracy of the algorithm.

3.2. Comparison of results from different methods

To compare the accuracy of the different methods, the following four methods are used to measure the particle motion in the simulated flow field: pyramid optical flow PTV (P-PTV), which involves a direct detection of the overall non-uniform granular flow field; vortex region segmentation pyramid optical flow PTV (VRSP-PTV), an empirical segmentation method, which divides the flow field into several localized regions containing vortex centers based on the position of the vortex, and then measures the velocity of the particles in the sub-regions; horizontal velocity segmentation PyrLK-based PTV (HVSP-PTV), which divides the region by level set partitioning based on the distribution characteristics of the horizontal velocity field and finally measures the velocity of particle motion in each sub-region; and vertical velocity segmentation PyrLK-based PTV (VVSP-PTV), which divides regions based on the distribution characteristics of the vertical velocity field and measures the velocity of particle motion in each sub-region.

Figure 7 shows the results of velocity field segmentation using VRSP-PTV, HVSP-PTV, and VVSP-PTV. The red arrow in Fig. 7(a) represents the velocity of the particle, and the blue dashed line represents the boundary of the region directly divided based on the position of the vortex. Figures 7(b) and 7(c) are pseudo-color images of the horizontal and vertical velocities, respectively. The white solid lines in the images represent the regional boundaries segmented and smoothed according to the horizontal and vertical velocity fields, respectively.

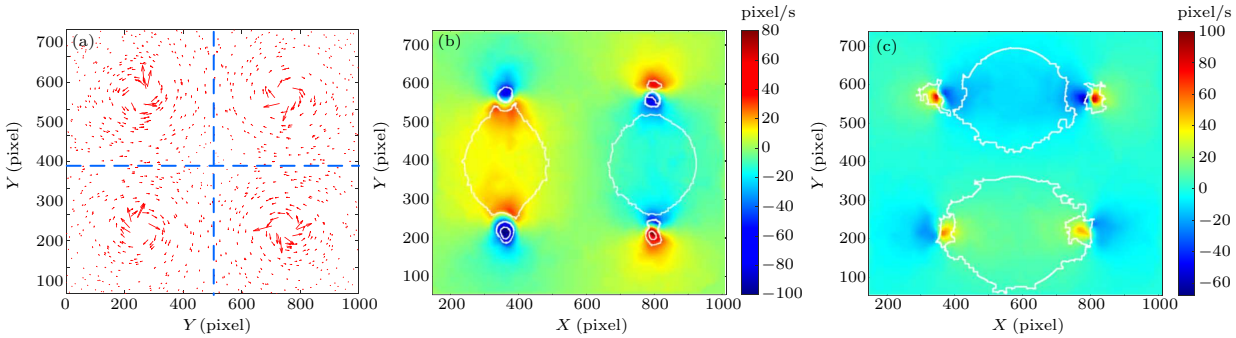


Fig. 7. Simulation of vortex field segmentation. (a) Vortex position segmentation. (b) Horizontal velocity field segmentation. (c) Vertical velocity field segmentation.

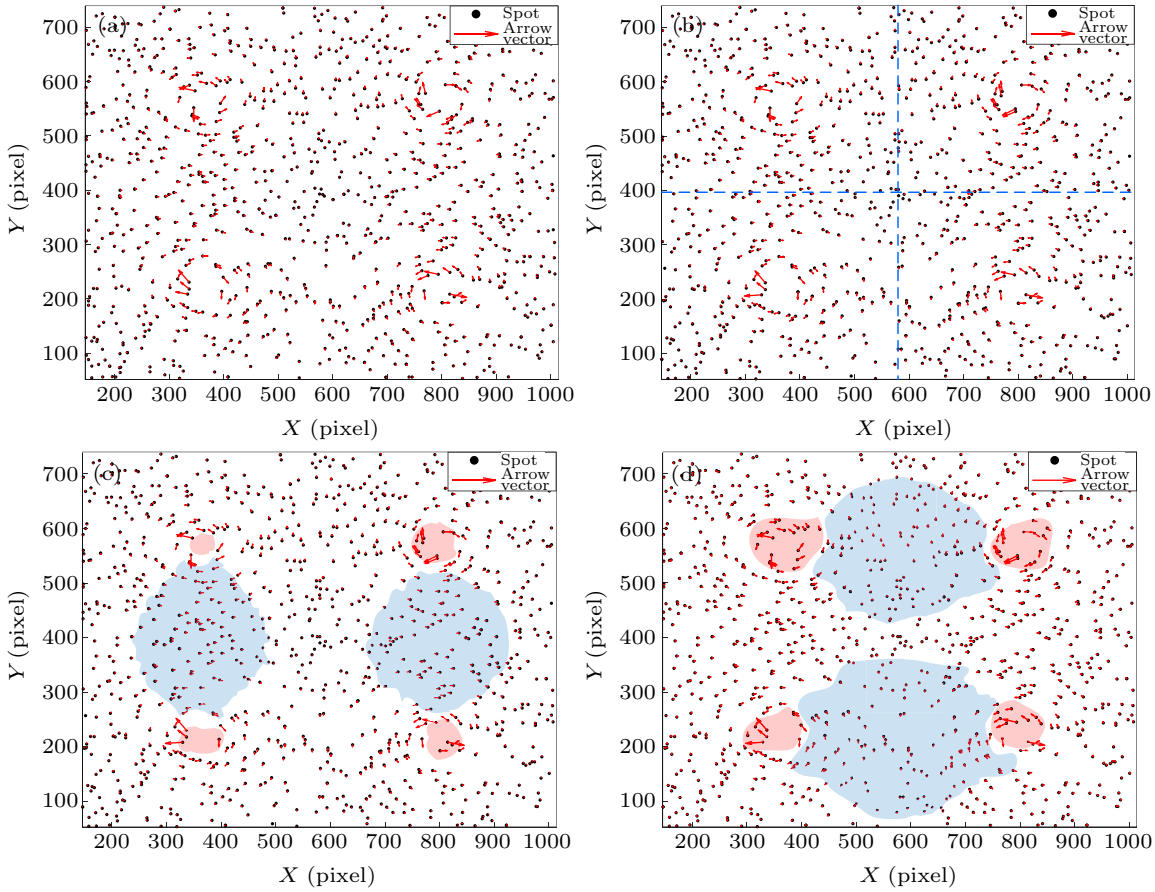


Fig. 8. Velocity fields obtained from the four measurement methods: (a) P-PTV, (b) VRSP-PTV, (c) HVSP-PTV, and (d) VVSP-PTV. The blue dashed lines in the figure delineate the areas, and the colored areas indicate the segmented areas.

Figure 8 shows the velocity field at a specific moment obtained from the simulated flow field using the four methods: P-PTV, VRSP-PTV, HVSP-PTV, and VVSP-PTV. The black dots represent the individual particles, and the red arrows represent the velocities of the corresponding particles. Figure 8(a) shows the measurement results of the P-PTV method, which does not segment the region and directly measures the overall flow field. Figures 8(b)–8(d) show the velocity field obtained by first dividing the region using three different partitioning methods (as shown in Fig. 7) and then measuring the segmented area.

Statistical analysis was performed on the measurement results, and the measurement accuracies of the different methods were calculated using the following formula:

$$\eta = \left[1 - \xi \cdot \frac{\sum_{i=1}^{M} \sqrt{\left(\frac{s_i - p_i}{D_{\mathrm{m}}}\right)^2 + \left(\frac{t_i - q_i}{D_{\mathrm{n}}}\right)^2}}{M}\right] \times 100\%, \quad (9)$$

where M denotes the total number of particles detected in the image; (p_i, q_i) are the real coordinates of particle i in the simulated flow field; and (s_i, t_i) are the measured coordinates of particle i. D_{m} and D_{n} represent the width and height of the simulated system area, respectively. ξ is a constant factor with a value of 0.9, used to adjust the impact of errors and tune the results of the formula according to practical needs.

The duration of the simulating flow field is 1 s, with a time interval of 0.005 s per frame. The particle velocity accuracy in the different methods at different times within 1 s was obtained. To depict the change in accuracy over time more clearly, the accuracy for every 10 frames was averaged to represent an accuracy over 0.05 s, as shown in Fig. 9.

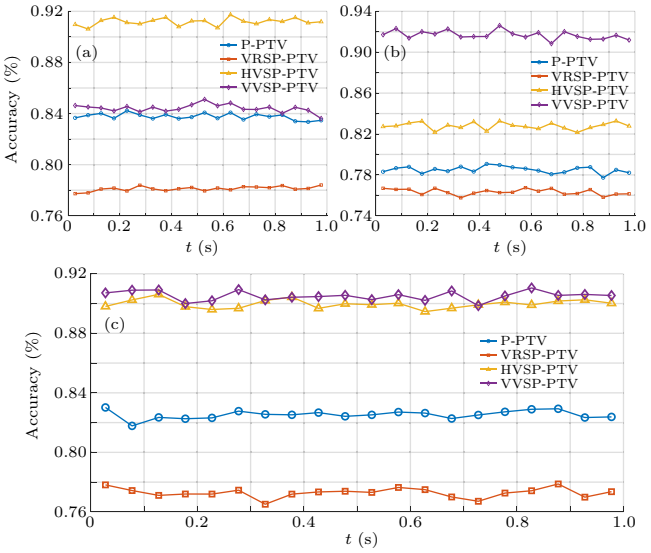


Fig. 9. Accuracy of methods at different times. (a) Accuracy of v_x. (b) Accuracy of v_y. (c) Accuracy of v.

The above images show that the accuracies of the HVSP-PTV and VVSP-PTV methods were higher than those of the P-PTV and VRSP-PTV methods. In addition, the VVSP-PTV method achieved the highest accuracy for v_y, whereas the HVSP-PTV method achieved the highest accuracy for v_x. Table 1 shows the average accuracy of the four methods.

Table 1. Average accuracy of several methods.

Methods	P-PTV	VRSP-PTV	HVSP-PTV	VVSP-PTV
v accuracy	82.53%	77.29%	89.97%	90.52%
v_y accuracy	78.50%	76.33%	82.79%	91.68%
v_x accuracy	83.76%	78.12%	91.18%	84.41%

The accuracy of the four methods was calculated based on the differences between the measured and actual particle coordinates. Table 1 presents the calculation results for the accuracy of the four different methods, including the accuracy of the combined velocity v, horizontal velocity v_x, and vertical velocity v_y. For the combined velocity v, the accuracies of the HVSP-PTV and VVSP-PTV methods were higher than those of the P-PTV and VRSP-PTV methods, with the VVSP-PTV method showing the highest accuracy of 90.52%. The VRSP-PTV method had the lowest accuracy for the combined velocity v, indicating that segmentation based on vortex position was not reasonable. Furthermore, it can be observed that using the level set segmentation method to divide the horizontal and vertical velocity fields into regions and measure them can significantly improve the accuracy of particle velocity detection. In addition, the accuracy of the HVSP-PTV method for v_x was 91.18%, which was higher than that of the VVSP-PTV method, and the accuracy of the VVSP-PTV method for v_y was 91.68%, which was higher than that of the HVSP-PTV method.

4. Experiments in silo granular flow

Because of the narrowing at the outlet of the silo, as well as the energy dissipation caused by collision and friction between particles,[31] a conical region is formed in which internal movement of particulate materials occurs in the silo, resulting in a dynamic non-uniformity of dense particle flow inside the silo.[32] Moreover, the particles in the silo are characterized by a large number of targets and a large velocity gradient. Therefore, there is a high demand for measurement technology, and the applicability of the proposed method in a dense granular flow field can be verified in the silo. A high-speed camera was used to record the process of particle motion, and the positions of the particles in the image were then analyzed and tracked to obtain their velocities.[33] Figure 10 shows a diagram of the experimental setup for measuring particle flow in a silo. The experimental system included four main parts: a high-speed camera, an LED light source, a three-dimensional semi-cylindrical silo, and spherical particles.

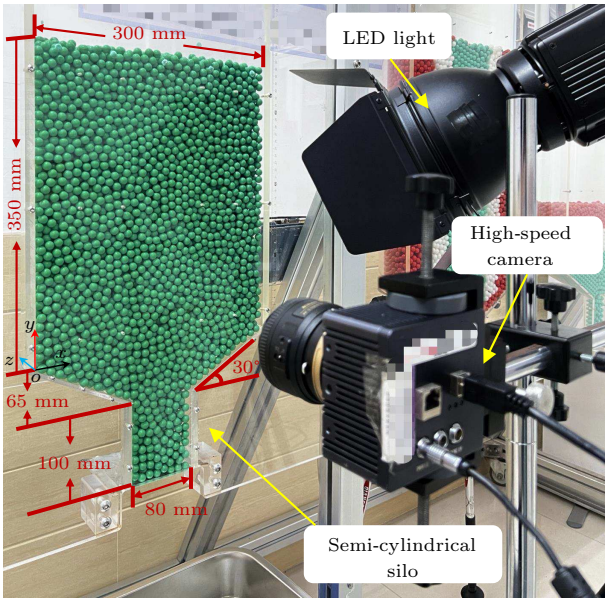


Fig. 10. Experimental setup for measuring particle flow in a silo.

(i) Experimental setup and particle material The three-dimensional semi-cylindrical silo was made of transparent organic glass with a thickness of 10 mm, cross-sectional diameter of 300 mm, outlet width of 80 mm, and a cone angle of 30°. A channel with a length of 100 mm was installed at the outlet to prevent particle splashing. The experimental particles were POM particles with a size of 10 mm.

(ii) Camera and light source The model of the high-speed camera was 5F04. Its exposure time and frame rate were set to 800 μs and 200 Hz, respectively. The LED light source was an SL-200W, which had an output of 200 lumens.

A spatial right-angled coordinate system was established in the three-dimensional silo, as shown in Fig. 10, with the intersection of the back of the silo, left boundary of the cylinder, and bottom section of the cylinder as the coordinate origin *o*. The plane formed by the *x*- and *y*-axes was parallel to the front wall of the silo, and the horizontal backward direction was the positive *z*-axis direction. Before the experiment, the outlet was blocked with a wooden board, and the center loading method was used to fill the particles.[34] The height of the particle stacking was 350 mm, the wooden board was opened for unloading, and a high-speed camera was used for 25 s to continuously capture pictures of the particle motion.

4.1. Velocity field distribution

4.1.1. Measurement results

Figure 11 shows the segmentation and measurement results for the velocities of discrete particles in the silo during unloading using the HVSP-PTV and VVSP-PTV methods. In other studies, when the wooden board was opened for unloading, the stress in the particle system changed suddenly,[35] leading to the emergence of a vortex structure in the silo in the local high-shear region.[36] However, this phenomenon was not observed in the current experimental measurements. Therefore, we collected images of the particle motion during the first 1.5 s after opening the orifice. First, 20 images were selected at equal time intervals, the motion velocity of the particles was measured using the traditional optical flow method, average processing was carried out to obtain the average velocity distribution, and the average velocity field was processed using the level set segmentation method. The results are shown in Figs. 11(a) and 11(b). In the figure, the velocity of particles in the red region I, yellow region II, and green region III decreases sequentially, and the particle velocity tends to be the same within each region. Thus, the segmentation ensures the uniformity of the particle motion velocity within the sub-regions.

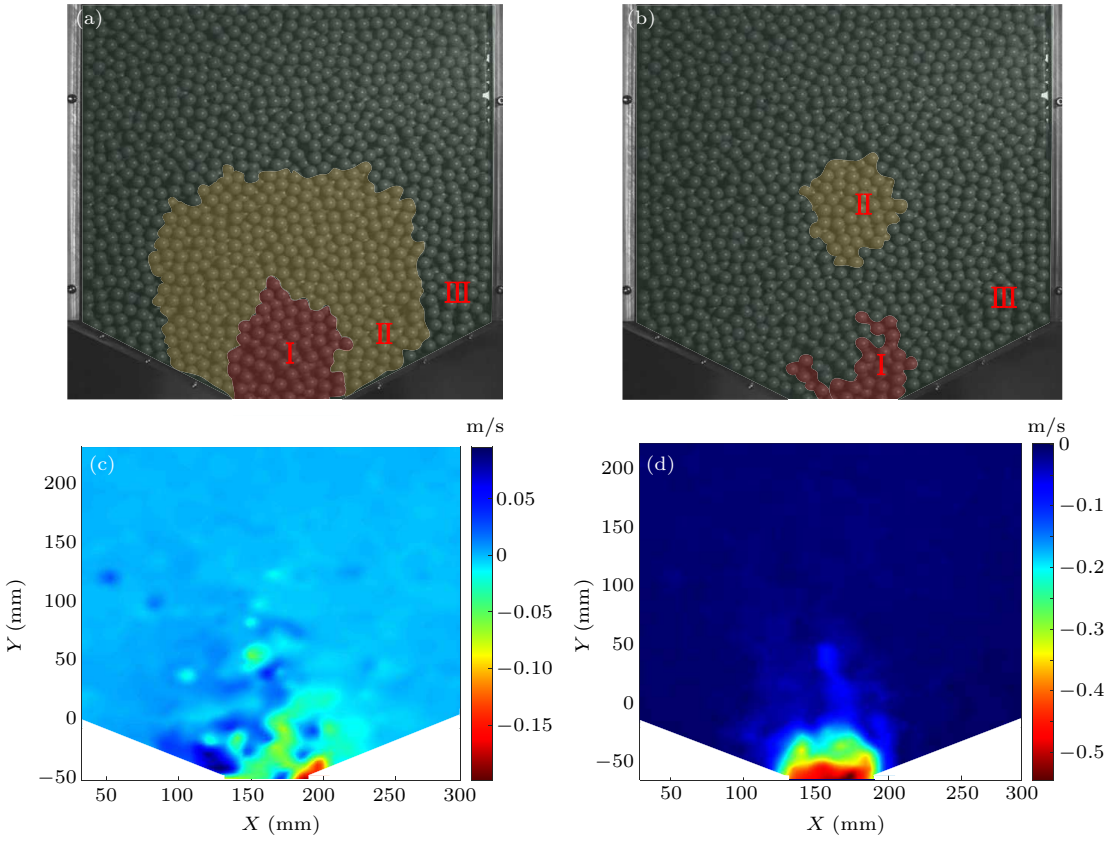


Fig. 11. Silo field segmentation results and measurement results. (a) Results of the horizontal velocity field segmentation of particles in the silo. (b) Results of the vertical velocity field segmentation of particles in the silo. (c) Pseudo-color map of horizontal velocity after field segmentation. (d) Vertical velocity pseudo-color map after field segmentation. As the color changes from red to yellow to green to blue, the speed decreases successively.

Figure 11(a) shows the results of segmenting the horizontal velocity, in which red region I is not adjacent to yellow region II, which is closer to the middle of the silo, and the remaining region is green region III. Figure 11(b) shows the results of segmenting the vertical velocity, in which regions I, II, and III are adjacent to each other in order, with red re-

gion I located above the outlet and green region III furthest away from the outlet. Figures 11(a) and 11(b) show that there is a significant difference between the segmentation results of the horizontal and vertical velocities. This is because during the unloading process of the silo, the particles are affected to varying degrees by gravity, friction, and interparticle interaction forces. In the vertical direction, the particles are mainly driven by gravity, which accelerates their descent, resulting in a gradual increase in vertical velocity, whereas in the horizontal direction, the particles are mainly affected by friction and interactions between them, but not by gravity, resulting in an uneven horizontal velocity distribution of the particles, as shown in Fig. 11(a).

Figures 11(c) and 11(d) show the pseudo-color images of particle motion velocity at $t = 0.9$ s after the start of unloading. Figure 11(c) shows the horizontal velocity distribution obtained by the measurement based on the segmentation results in Fig. 11(a). The velocity distribution in the region above the outlet is asymmetric, with the high-velocity region on the right and the low-velocity region on the left. This shows that the horizontal velocity distribution of the particles was not even at the time of measurement, reflecting the disorder of the silo particle system.[37,38] Figure 11(d) shows the measured vertical velocity distribution based on the segmentation results in Fig. 11(b). It can be observed that the closer a region is to the outlet, the darker red its color; that is, the closer the particles are to the outlet, the larger their velocity value. The farther a region is from the outlet, the darker blue its color; that is, the farther away the particles are from the outlet, the smaller their velocity. The main reason is that particles near the outlet are subjected to gravity and rapidly accelerate downwards, gaining a large vertical velocity, whereas the particles farther away from the outlet are more tightly distributed and are subjected to collision, support, and friction between the discrete particles, resulting in very small acceleration. Therefore, their velocities are much smaller than those of the particles near the outlet, which is a common manifestation of the velocity gradient under gravity.[39]

4.1.2. Vortex motion

Furthermore, a brief vortex motion of the particles in the region above the silo outlet near the side wall was detected at a time of 1.5 s after unloading. Figure 12 shows a velocity map of the particles in the silo obtained using the modified optical flow method, with hollow circles representing the particles and colored arrows representing their velocities. By calculating and analyzing the velocity field of the particles during the first 1.5 s of unloading from the silo, the vortex motion of discrete particles near the purple arrow was found to occur within 1.17 ± 0.005 s.

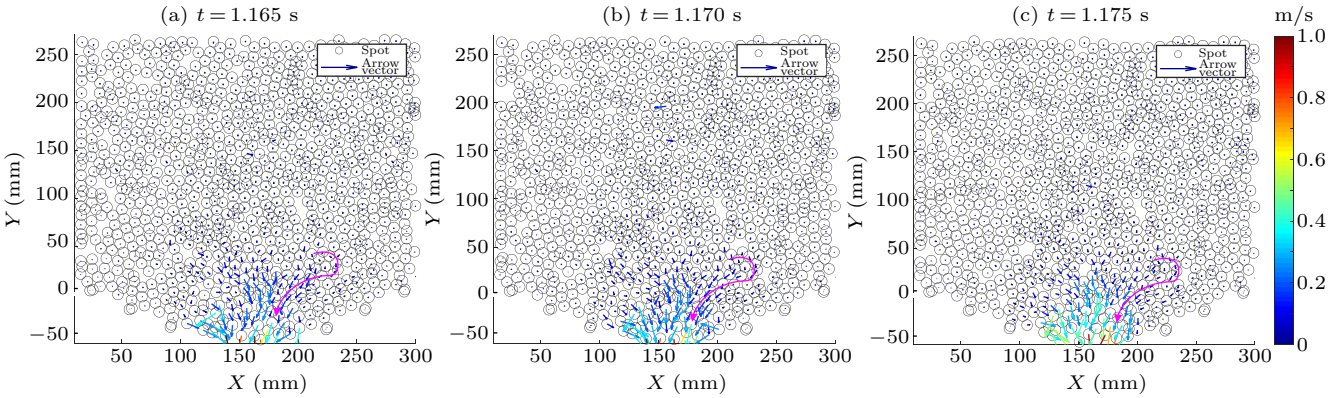


Fig. 12. Velocity vector.

4.1.3. Velocity distribution

Figure 13 shows the statistical results of the velocity field distribution of the particles at different moments during the unloading process of the silo obtained using the optical flow method applied after the level set segmentation method. Owing to the unstable state of the particle movement in the early stage of unloading, the velocity changes were large, and the measurements were performed after the flow of particles in the silo was stabilized. Four moments when the particles were at different heights during the unloading process of the silo were selected ($t = 6$ s, 9.75 s, 13.5 s, and 17.25 s) for statistical analysis. Each time interval was 3.75 s long, and different colors were used to represent the velocity distribution of the particles in the silo at these four times.

The motion of a single particle is random; therefore, it is necessary to divide the measurement area to calculate the velocity distribution of the particle flow. To ensure consistency in the motion of discrete particles within the measurement area, the division width was considered equal to the outlet width, which was 80 mm. To ensure that each small, partitioned area contained at least one particle, a partition height of 20 mm was used. Finally, the average velocity of the particles within each 80 mm × 20 mm area was calculated as the velocity value corresponding to height, as shown in Fig. 13(a). The least-squares

method was used for fitting the data, and the velocity distribution of the granular flow was found to conform to an exponential function within an error range of less than 5%. The velocity distribution of the granular flow was consistently independent of time, and the particle velocity at the exit of the silo ($y = -65$ mm) was concentrated at 0.35 m/s. With an increase in the silo height, the velocity of the particle motion decreased, which is consistent with the measurement results of Song.[20]

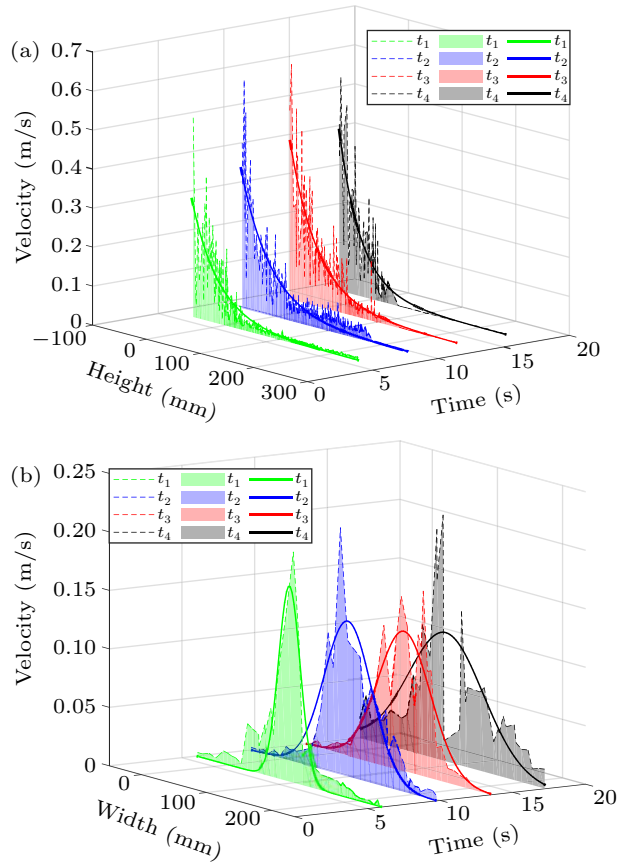


Fig. 13. Velocity distribution at different moments using the improved P-PTV method. (a) Velocity distribution at different heights and (b) velocity distribution at the same horizontal altitude.

To ensure that the motion of the discrete particles in the measurement area contained multiple characteristic regions (fast flow, slow flow, and quasi-stationary), particles located at a height of 65–75 mm in the silo were selected with a height of 10 mm. To ensure that each small area contained at least one particle, a partition width of 30 mm was used. Finally, the average speed of the particles in each 30 mm $\times$ 10 mm area was calculated as the velocity at the corresponding position, as shown in Fig. 13(b). Using the least-squares fitting process, the velocity distribution of the granular flow was found to conform to a Gaussian function with an error of less than 5%. It can be seen that the velocity distributions of the granular flow at the four moments are consistent, and the particle velocity at the central point directly above the silo outlet ($x = 150$ mm, $y = 0$ mm) was the highest, and it decreased as it approached the edge wall of the silo, which is consistent with the measurement results of Wang.[13] This is mainly because at the same horizontal height, the particles in the center position are located directly above the silo outlet and are subject to less resistance.

5. Conclusion

In this study, an improved particle tracking velocimetry method is proposed, which mainly uses the level set segmentation algorithm to obtain the boundary contour of the region with large velocity gradient changes and divides the inhomogeneous flow field into regions according to the boundary contour to obtain sub-regions with uniform velocity distribution, and then utilizes the particle tracking velocimetry method based on optical flow to measure the velocities of the discrete particles in each sub-region to avoid the phenomenon of over-smoothing.

The accuracy of the algorithm was verified by simulating a complex flow field containing both rotational and translational motions. The following four methods were compared: P-PTV, VRSP-PTV, HVSP-PTV, and VVSP-PTV. The results show that the improved particle tracking velocimetry method can achieve an accuracy of 90%, which is an improvement of approximately 10% compared to the P-PTV method. Subsequently, we applied the improved method to practical scenarios to measure the velocity field of the dense granular flow in a silo during unloading. Vortex structures were experimentally observed at 1.17 ± 0.005 s in the region above the silo outlet. During the steady-state flow stage, the axial velocity distribution of the dense granular flow in the silo satisfied an exponential function distribution, and the radial velocity distribution satisfied a Gaussian function distribution. The experimental data show that the improved particle tracking velocimetry method can be applied to measure the motion state of a silo–particle system, which verifies the practicality of this method in granular flow fields.

References

[1] Major J J 2000 *J. Sediment. Res.* **70** 64
[2] Zhou H 2014 *Numerical simulation and experimental study of pharmaceutical fluidized bed particle preparation process* (Ph.D. Dissertation) (Beijing: University of Chinese Academy of Sciences)
[3] Xia J X, Ni J R and Huang J Z 2002 *Min. Metall. Eng.* **22** 37
[4] Koh C A, Sloan E D and Sum A K 2011 *Natural Gas Hydrates in Flow Assurance* (Oxford: Gulf Professional Publishing)
[5] Yang H, Zhang G H, Wang Y J and Sun Q C 2018 *Adv. Mech.* **48** 541
[6] Arévalo R and Zuriguel I 2016 *Soft Matter* **12** 123
[7] Zhu H P and Yu A B 2004 *J. Phys. D: Appl. Phys.* **37** 1497
[8] Chen Q 2021 *Multi-scale measurement and study of particle flow dynamics characteristics in silos* (Ph.D. Dissertation) (Shanghai: University of Shanghai for Science and Technology)
[9] Xu Y, Zeng Q, Li R, Chen Q, Li Y M and Mu T T 2024 *J. Univ. Shanghai Sci. Technol.* **46** 171
[10] Hsiau S S and Jang H W 1998 *Therm. Fluid Sci.* **17** 202

[11] Sielamowicz I, Blonski S and Kowalewski T A 2005 *Chem. Eng. Sci.* **60** 589
[12] Sielamowicz I, Blonski S and Kowalewski T A 2006 *Chem. Eng. Sci.* **61** 5307
[13] Wang B D, Song J, Li R, Han R, Zheng G and Yang H 2020 *Chin. Phys. B* **29** 014207
[14] Zhou Y X 2019 *Acta Phys. Sin.* **68** 134701 (in Chinese)
[15] Liu S, Zhou Z, Zou R, Pinson D and Yu A B 2013 *AIP Conf. Proc.* **1542** 694
[16] Yang S Q and Chow A T 2008 *Adv. Water Resour.* **31** 1344
[17] Lu J, Yang H, Zhang Q H and Yin Z P 2019 *Exp. Fluids* **60** 10
[18] Yang H, Shi H, Lu J, Kang M and Yin Z 2021 14*th International Symposium on Particle Image Velocimetry* **1** 1
[19] Zhou Y L, Song L Z and Zhou H J 2011 *J. Chem. Eng.* **62** 348
[20] Song J, Yang H, Li R, Chen Q, Zhang Y J, Wang Y J and Kong P 2019 *Powder Technol.* **355** 172
[21] Peng X X, Luo X and Han B L 2022 *Comput. Appl. Softw.* **39** 241
[22] Bruhn A, Weickert J and Schnörr C 2005 *Int. J. Comput. Vis.* **61** 211
[23] Lucas B D and Kanade T 1981 *7th International Joint Conference on Artificial Intelligence*, August 24–28, Canada, 1981, p. 674
[24] Lu J 2021 *Velocimetry of variable spectral flow particle images in hypersonic flow field* (Ph.D. Dissertation) (Wuhan: Huazhong University of Science and Technology)
[25] Shah D M J and Mumford D 1989 *Comm. Pure Appl. Math* **17** 577
[26] Cremers D, Rousson M and Deriche R 2007 *Int. J. Comput. Vis.* **72** 195
[27] Wali S, Li C M, Imran M, Shakoor A and Basit A 2023 *Signal Process.* **211** 109105
[28] Monzón N, Salgado De La Nuez A and Sánchez J 2016 *Img Process On Line.* **6** 165
[29] Baumgart A and Blanquart G A 2023 *J. Comput. Phys.* **491** 112353
[30] Bukreev F, Raichle F, Nirschl H and Krause M J 2023 *Chem. Eng. Sci.* **270** 118485
[31] Du T J, Zhou L, Chen L F, Wang H J, Chen Q and Kong P 2023 *China Powder Sci. Technol.* **166** 40
[32] Nielsen J 1998 *Philos. Trans. R. Soc. London, Ser. A* **356** 2667
[33] Ran T, Madelyn W and Eric R W 2021 *Phys. Rev. E* **104** 044909
[34] Horabik J, Parafiniuk P and Molenda M 2016 *Biosyst. Eng.* **149** 60
[35] Wang Y, Lu Y and Ooi J Y 2015 *Powder Technol.* **282** 43
[36] Tewari S, Dichter M and Chakraborty B 2013 *Soft Matter* **9** 5016
[37] Maiti R, Das G and Das P K 2017 *Phys. Fluids* **29** 10
[38] Xiao Y W 2022 *Study on the behavior of particle dynamics during silo unloading* (Ph.D. Dissertation) (Haerbin: Northeast Agricultural University)
[39] Gella D, Maza D and Zuriguel I 2017 *Phys. Rev. E* **95** 052904